International Journal of Information, Control and Computer Sciences
ISSN: 2517-9942
Vol:14, No:10, 2020

Artificial Intelligence-Based Chest X-Ray Test of COVID-19 Patients

Dhurgham Al-Karawi, Nisreen Polus, Shakir Al-Zaidi, Sabah Jassim

***Abstract*—**The management of COVID-19 patients based on chest imaging is emerging as an essential tool for evaluating the spread of the pandemic which has gripped the global community. It has already been used to monitor the situation of COVID-19 patients who have issues in respiratory status. There has been increase to use chest imaging for medical triage of patients who are showing moderate-severe clinical COVID-19 features, this is due to the fast dispersal of the pandemic to all continents and communities. This article demonstrates the development of machine learning techniques for the test of COVID-19 patients using Chest X-Ray (CXR) images in nearly real-time, to distinguish the COVID-19 infection with a significantly high level of accuracy. The testing performance has covered a combination of different datasets of CXR images of positive COVID-19 patients, patients with viral and bacterial infections, also, people with a clear chest. The proposed AI scheme successfully distinguishes CXR scans of COVID-19 infected patients from CXR scans of viral and bacterial based pneumonia as well as normal cases with an average accuracy of 94.43%, sensitivity 95%, and specificity 93.86%. Predicted decisions would be supported by visual evidence to help clinicians speed up the initial assessment process of new suspected cases, especially in a resource-constrained environment.

***Keywords*—**COVID-19, chest x-ray scan, artificial intelligence, texture analysis, local binary pattern transform, Gabor filter.

I. Introduction

THE SARS-CoV-2 pandemic continues to wreak havoc across the world in a manner unwitnessed since the unusual deadly influenza's pandemic of 1918, otherwise known as the Spanish flu. Since December 2019 to June 2020, over 8.8 million confirmed cases were globally reported [1]. The century long advances in science, medicine and technology facilitated the rapid emergence of a globally adopted strategy to confront the enormity of COVID-19 challenges to ensure significantly lower level of casualties. This strategy is based on (a) developing faster and more accurate diagnostic methods, (b) conducting clinical trials on possible drug treatments, and (c) developing appropriate vaccines. With the increasing spread of the disease and the nature of the outbreak, the highest priority is to scale up public health testing while developing new means of testing.

Molecular diagnosis of COVID-19 using real-time RT-PCR test is the preferred screening/testing method [2]. While laboratory-based performance evaluations of RT-PCR test show high analytical sensitivity and near-perfect specificity with no misidentification of other coronaviruses or common respiratory pathogens, test sensitivity in clinical practice may be adversely affected by a number of variables including adequacy of specimen, specimen type and handling, stage of infection (The Centers for Disease Control and Prevention (CDC) guidelines for *in vitro* diagnostics). Indeed, early reports of test performance in the Wuhan outbreak showed variable sensitivities ranging from 37% to 71% [3], [4]. Concerns about test availability and delays in PCR test have led to promoting the use of serological tests for antibodies detection as proof of positive COVID-19 infection. Unlike the RT-PCR, these are not diagnostic tests but are meant to help estimate the proportion of the population that have had the infection and developed antibodies to it. Such tests are continually developed, manufactured, and made available in some countries. In April 2020 - Roche (SIX: RO, ROG; OTCQX: RHHBY) announced the development and upcoming launch of its Elecsys® Anti-SARS-CoV-2 serology test to detect antibodies in people who have been exposed to the Severe Acute Respiratory Syndrome Coronavirus 2 (SARS-CoV-2) that causes the COVID-19 disease. The newly formed Rapid Testing Consortium at Oxford University has been reported to be "close to picking up 100% of all cases where people have antibodies. Now it is just a question of scaling up the manufacturing process." [5] However, recently doubts have been raised about the reliability of antibody tests. According to WHO, only a tiny proportion of the global population – maybe as few as 2% or 3% – appear to have antibodies in the blood showing they have been infected with COVID-19. Interested readers can find more on these issues from a variety of web reports (e.g. see [6], [7]). Detecting a high-level level of antibodies in the blood does not show "that an individual is immune or is protected against re-infection".

This paper is concerned with a third significant and complimentary line of emerging investigations that targets the use of Artificial Intelligence (AI) based efficient classification to analyze radiology chest scan images of suspected patients. The paper is structured as follows. Section II explains the related work. Section III describes the proposed schemes, while Section IV presents the experimental results and discussion. Section V concludes the existing study and illustrates some opportunities for future work.

II. Related Work

Radiographic chest scans with CXR and CT images, as key tools for pulmonary disease diagnosis and management, form a useful source of complementary tools for testing and

Dr. Dhurgham Al-Karawi, Dr. Nisreen Polus, Dr. Shakir Al-Zaidi, are with the Medical Analytica Ltd, Flint, CH6 5XA, UK (corresponding author, phone: +44(0)1244833961; e-mail: Dhurgham@medicalanalytica.co.uk).

Sabah Jassim is Professor of Mathematics at the University of Buckingham, England, MK18 1EG, UK and adviser to Medical Analytica Ltd.

management purposes in dealing with COVID-19 pandemic. Since the emergence of the disease in Wuhan, China, there has been a growing number of investigations in this direction, evidence of their use across the different diagnosis and management scenarios have been noted as of 1st April 2020, in [8], as yet scant and may undergo refinement through rigorous scientific investigation. Guided by high clinical suspicion and laboratory assessment of COVID-19 suspected cases, radiographic imaging has been used to guide patient management decisions in categories of self-isolation at home, admission and isolation or evaluation for alternative diagnoses [9] and a similar process has been used in Spain. Classic CXR findings in COVID-19 are multiple, bilateral, or unilateral, peripheral ground glass opacities. Organizing pneumonia patterns and crazy-paving patterns may be present [10]. Due to the wide availability of conventional chest radiography units, especially the mobile ones, and the ease of decontaminating the equipment between patients has given CXR an essential role in the fight against this pandemic. In order to support radiologist to perform such tasks, some research groups have developed Deep learning/Transfer learning techniques to analyze CXRs and classify them into COVID-19 and non-COVID (normal CXR); however these algorithms have achieved varying results [11], [12].

On 11th April 2020, Ilyas et al. [13] presented a review of several early AI-based deep learning systems designed for the automatic detection of COVID-19 from CXR. The reported schemes are trained on different size datasets primarily to detect pneumonia as an indicator of COVID-19. With two exceptions, all achieve considerable-to-impressive accuracy rates of 80%-98%. The review concludes that all those AI approaches are detecting the subjects suffering with pneumonia without determining whether the pneumonia is caused by COVID-19 or due to any other bacteria or virus. In most cases, the training and testing datasets are rather small size. This is a known source of overfitting by deep learning schemes besides the black-box style of their decisions.

The main contribution of this paper is the development of innovative AI schemes for the analysis of CXR images on a combined dataset comprising CXRs of positive COVID-19 patients, patients with various viral and bacterial infections, as well as people with a clear chest. Instead of developing deep learning models, we opt for certain types of texture analysis that allow an informative way of justifying the output decisions. This paper is a follow up on our recent work [14], on the analysis of chest CT scan images of Coronavirus (COVID-19) patients, and building on our accumulated experience on developing computer aided diagnosis for tumor analysis, we shall promote the innovative idea of texture analysis in the frequency and other transform domains.

III. The Proposed CXR Based COVID-19 Recognition Algorithm

A computer-based system for categorizing CXR scan images is expected to add an innovative digital test to complement and improve the performance of existing diagnostic tests for detecting COVID-19 infection in suspected patients. Integrating an AI-based approach into clinical practices of the RT-PCR and/or the growing number of developed antibody tests should aim to better accuracy of positive detection, and hence greatly reduce the false-negative rate and improve the true positive rate. In computer vision, two different AI approaches have been dominating the research endeavor in this field, namely deep learning (DL) and what is loosely termed as hand-crafted feature analysis. Both share the common 2-steps strategy of extracting what is known as a "feature map" image representation followed by the use of a data classifier, and they differ only in where to put most efforts. In the DL approach, the emphasis is on extracting a feature map that encapsulates as many as possible image local features whereas the non-DL approach creates a feature map consisting of one or more known/meaningful features. DL schemes require a large number of samples for training and the outcome suffers more than the non-DL schemes from overfitting [15]. In this paper, we continue to opt for non-DL approach. This is motivated by the success in our earlier work [14] on using CT scans to test for COVID-19 infection, and is justified by research done by the first and last authors, on classifying Ultrasound Ovarian Tumors by AI texture analysis schemes [16], [17]. The innovative contribution of the current paper is to extend the practice of extracting image texture features from the Fourier domain into another known image transform domain, namely the Local Binary Patterns (LBP).

Our proposed AI scheme for distinguishing CXR images of COVID-19 patients from those of patients who are uninfected (i.e. normal) or infected by other viral or bacterial diseases, will be based on extracting texture features that exhibit noticeable patterns of variation relating to COVID-19 infection progression. The scheme follows the typical framework of non-deep machine learning scheme for image classification that works by (a) pre-processing the image using adaptive winner filter [14] for noise reduction and image quality improvement, followed by inversion, (b) applying the LBP transform, (c) selecting a texture type and extracting the appropriate feature vector, and (d) training and testing the performance of each scheme on a sufficiently large dataset of image, using the linear Support Vector Machine (SVM) classifier [18].

A. Characterizing Texture Features in CXR Scans of COVID-19 Patients

Image features refer to pixel intensity patterns or quantitative data values that reveal meaningful information about image pixels in terms of local and/or global variations. Feature extraction is the process of determining a feature vector representation of input images, and effectively isolating the most critical attributes relevant to the aim of the intended application. Popular image analysis features include color, color distributions, color variation patterns from different domains (spatial or frequency domain) of an image [19]. Image-texture often refers to repeated patterns of pixel intensity value changes, and texture is accepted as a unifying approach to analyzing a wide range of image types (natural, biometrics, satellite, etc.) for various tasks including segmentation, object detection/tracking, and classification.

In the classification of CT scan images of COVID-19 [14], it was found that textures extracted from the Fourier transform (FFT-spectrum) provided the most COVID-19 distinguishing features. Fourier transform is a mathematical tool that represents data signals/images in terms of waveforms of different frequencies, and when applied to image data its frequency content is analyzed into different ranges. Higher frequency ranges are associated with more significant texture components. The FFT spectrum quantifies the presence/ strength of various frequencies.

Based on the success of the FFT-Gabor texture in achieving high accuracy for CT-based analysis, we first tested the performance of this feature for the intended scheme only to find that it performed well but not as good as its performance with CT scan. Therefore, we opted to extract texture features from the LBP transform domain. The LBP transform acts as a non-linear filtered version of the image. Each pixel is replaced by a byte representing the order relation between the pixel value and its 8-immediate neighbors scanned in a clockwise manner starting from to top left corner. If the neighbor is ≥ than the center pixel value, then the corresponding bit is set to 1 otherwise it is set to 0, see Fig. 1 for an illustration. While each pixel in the LBP image depends on the neighboring 8 pixels. Besides being efficient, the LBP transform is invariant to illumination (i.e. unaffected by global grey-level increase/ decrease).

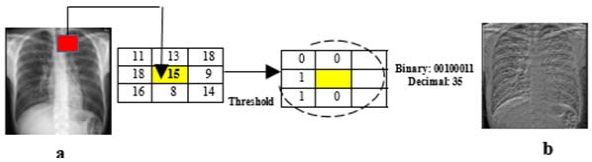

Fig. 1 (a) Input Image with a single LBP code from 3x3 block; (b) the LBP transformed image

We extracted various types of texture features from the LBP transformed images, but here, we shall only briefly describe the best three COVID-19 discriminating texture features as described in the following sections:

1) *Gabor texture feature:* Images are transformed by a set of parametrized 2-dimensional band-pass Gabor wavelet filters designed for detecting specific frequency information within an image region at a user chosen set of scales and orientation ranges [20]. The extracted Gabor-texture quantifies the frequency content in the input image within the sub-regions determined by the selected scales and directions.
2) *Uniform LBP (59 bins*): In many image analysis and pattern recognition applications, the 256-bins histogram of the LBP transformed images are used directly as a texture feature vector of the input images. Among the LBP codes, the uniform LBP (ULBP) codes (8-bit binary strings that contain single run of 1's, considered as a circular string) represent pixels with significant geometric textures. There are 58 ULBP's, and another way to form a texture feature vector representation of an input image, is a 59-bins histogram whereby the first bin is for the non-uniform LBP's and the remaining ones are for the 58 ULBPs [21].
3) *Histograms of Oriented Gradient (HOG):* The HOG is another localised texture-quantifying feature that has similarity with the Gabor filter features, but instead of applying a transform, it uses image gradient information (i.e. the rate of change between neighbouring pixels). The HOG feature, introduced in [22], works by subdividing the image into non-overlapping blocks of equal size and concatenate the histograms of oriented gradients in these blocks. The histograms are indicators of the location of intensity gradients and the edge directions in the image and provide information about the shape and presence of the structures contained within the image. The oriented gradient of an image *I* at pixel point *p(x,y)*, is the resultant of the horizontal vector:

$$gx = \left(I\left(p(x+1,y)\right) - I\left(p(x-1,y)\right)\right) \quad (1)$$

and the vertical vector is:

$$gy = \left(I\left(p(x,y+1)\right) - I\left(p(x,y-1)\right)\right) \quad (2)$$

The image I is then subdivided into non-overlapping rectangular cells of equal size. The oriented gradient of each cell is then organized into two matrices of the same cell size, one for orientation:

$$o = \arctan(g_{y/}g_x) \quad (3)$$

and the other for the magnitudes:

$$g = \sqrt{(g_x^2 + g_y^2)} \quad (4)$$

Each cell is then represented by a "9-bins histogram". The bins indices represent the nine orientation values {0, 20, 40, 60 … 160}. For each pixel of a cell, we locate the orientation of its gradient between two successive bins and split the magnitude to be added to these two bins proportionately. Finally, HOG is formed by concatenating the histograms of oriented gradients in these cells. The histograms are indicators of the location of intensity gradients and the edge directions in the image. The feature vector provides information about the shape and presence of the structures/objects within the image. In this study, images are subdivided into 16 rectangular cells, and HOG feature vectors size 144=9x16.

B. Performance Evaluation Framework of Our LBP-Based Schemes

This framework emulates a typical CAD process. It involves two key stages: training and testing. In the training stage, the feature vectors extracted from a sufficient number of samples will be used to determine the best separation of the extracted feature vectors by the chosen classifier model. Due to relatively high dimensionality of the various extracted texture feature vectors compared to the modest number of samples available for training, we choose the Linear SVM binary classifier. The

output from the SVM training stage is a hyperplane that separates the feature vectors of the positive class from those of the negative class.

In the testing stage, the feature vector of each testing image is extracted as usual and its signed distance from the SVM hyperplane is calculated, where predicted class is determined by the sign and actual distance is used to determine probability of the predicted class being accurate. Fig. 2 illustrates the full process of feature extraction applied to all images at the training as well as testing stages.

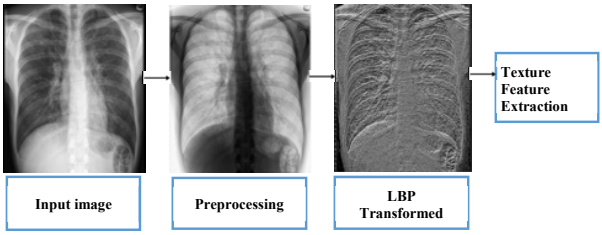

Fig. 2 Texture feature extraction in the LBP domain

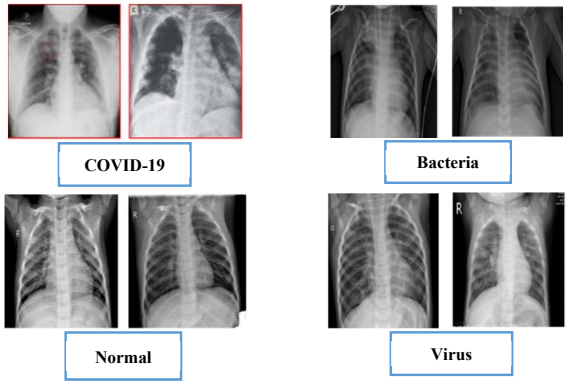

Fig. 3 Samples of CXR images in the experimental dataset

In this study, we shall conduct three different experiments: First, COVID-19 vs. Normal, Second, COVID-19 vs. Virus Infection & Bacteria, and the last experiment, COVID-19 vs. Normal, Virus Infection & Bacteria all together. To test the performance of the various LBP-based schemes, for the various combinations, we assembled an experimental dataset of 1015 CXR images obtained from two different sources: 305 images for COVID-19 were collected from [23], and 710 Images (Normal (305) + Viral Infection & Bacteria (405)) were collected from [24]. Fig. 3 displays samples from these different datasets.

While the COVID-19 transition is continuing, datasets of CXR images of newly examined COVID-19 patients will be frequently updated. These updates provide us with opportunities to update, improve and hopefully soon help achieve the best performance of our schemes independent of experimental datasets, and our experimental protocols are designed to be updatable as more data sample batches become available. Accordingly, we created a dataset of "prospective test" by isolating a set of 105 of COVID-19 images and for each of the three different experiments, and set aside 105 from the corresponding negative class as follows: first experiment 105 Normal CXR images, second experiment 105 Virus Infection & Bacteria images, third experiment 105 (35 Normal, 35 Virus Infection & 35 Bacteria) Images.

IV. Experimental Protocols' Classification Results and Discussion

For each experiment, we shall first train and test the performance of our LBP-based schemes with the remaining images of the corresponding dataset and follow the protocol described by the left side part of the self-explanatory block diagram of Fig. 4. At the end of these experiments, 30 SVM classifier models are output with its performance and the average of their accuracy/sensitivity/specificity rates are declared as the performance of the tested scheme. Subsequently, to test any new case, we use one of the 30 SVM hyperplanes namely the model with highest accuracy rate among those for which the difference between the sensitivity and specificity are minimal. This model will be used to test the performance of the scheme over the corresponding prospective testing data set, per the right-side diagram of Fig. 4.

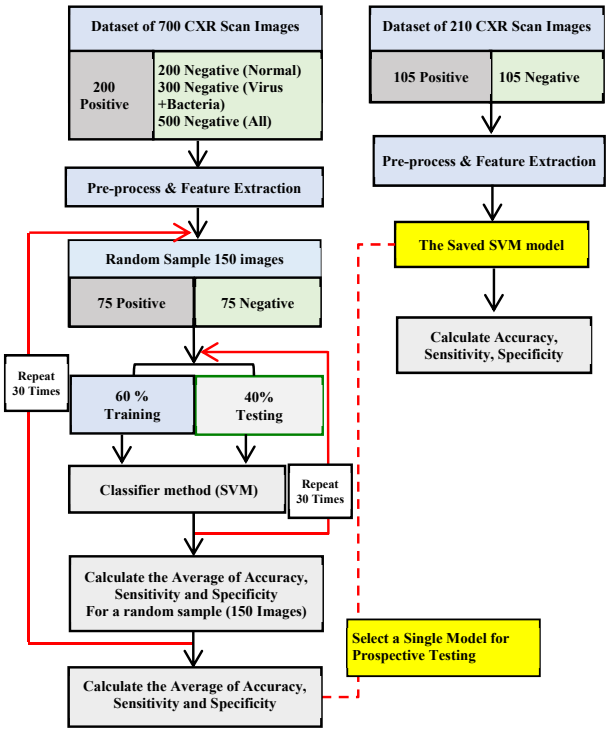

Fig. 4 Experimental protocols for both tests

Table I displays the results of the three experiments and includes the performance of the three different LBP-based texture COVID-19 classification schemes in terms of the average accuracy, sensitivity and specificity rates for the original training/testing experiments over the 700 images dataset. In each scenario, we also present the results of fusing the three texture schemes at the decision level using simple majority rule.

TABLE I
CLASSIFICATION RESULTS USING SVM CLASSIFIER

Texture Features.	Accuracy (μ)	Sensitivity (μ)	Specificity (μ)
COVID-19 VS. Normal			
LBP-Gabor.	97.16%	96.90%	97.43%
LBP-HOG.	92.83%	93.52%	92.15%
LBP-Uniform (59bins).	94.39%	95.29%	93.49%
Feature Fusion.	97.72%	97.89%	97.56%
COVID-19 VS. Viral Infection &Bacteria			
LBP-Gabor.	92.70%	93.36%	92.05%
LBP-HOG.	89.94%	90.20%	89.68%
LBP-Uniform (59bins).	90.72%	91.36%	90.08%
Feature Fusion.	92.77%	92.96%	92.59%
COVID-19 VS. Normal, Viral Infection & Bacteria all together			
LBP-Gabor.	94.15%	95.28 %	93.02 %
LBP-HOG.	90.87 %	91.03 %	90.71 %
LBP-Uniform (59bins).	91.14 %	90.74 %	91.55 %
Feature Fusion.	94.43%	95%	93.86 %

In Table II, we present the performance of the saved models over the corresponding 210 prospective datasets for the three scenarios including the majority rule fusion results.

TABLE II
CLASSIFICATION RESULTS USING SVM CLASSIFIER FOR PROSPECTIVE TEST

Texture Features	Accuracy (μ)	Sensitivity (μ)	Specificity (μ)
COVID-19 VS. Normal			
LBP-Gabor.	94.69%	95.24%	94.14%
LBP-HOG.	90.90%	91.86%	89.95%
LBP-Uniform (59bins).	92.88%	92.76%	91.01%
Feature Fusion.	95%	95.03%	94.98%
COVID-19 VS. Viral Infection &Bacteria			
LBP-Gabor.	90.92%	92%	89.85%
LBP-HOG.	87.7%	88.28%	86.12%
LBP-Uniform (59bins).	88.55%	89.72%	87.39%
Feature Fusion.	91.73%	92.85%	90.61%
COVID-19 VS. Normal, Virus Infection &Bacteria all together			
LBP-Gabor.	91.76%	92.36 %	91.17 %
LBP-HOG.	86.97%	88%	85.96%
LBP-Uniform (59bins).	90.18%	89.85%	90.52%
Feature Fusion.	91.95%	92.93%	91.01%

Overall, in each of the scenarios, Table I results show that each of the texture features has a significant power of discriminating images of COVID-19 from Normal, Virus Infection & Bacteria and all together individually. In each scenario, the LBP-Gabor scheme outperforms the other two texture schemes with the LBP-HOG being the lowest performing scheme but not by a significant amount. Perhaps, these results reinforce the widely accepted assertion that Gabor filters provide a credible mathematical model of the Human Vision system. Furthermore, each of the three texture schemes achieves the highest discrimination between CXR of COVID-19 patients against normal CXR images, and the lowest discrimination is achieved between COVID-19 against all others. Finally, although fusion of the three LBP-texture schemes resulted in improved performance, unfortunately only marginally. This may be explained as a shortcoming of the primitive majority decision rule rather than fusion in general, but it also reflects the superiority of the LBP-Gabor scheme which distinguishes COVID-19 CXR's from the normal, viral bacterial, and all cases with accuracy of 97.16%, 92.70%, and 94.15%, respectively. In all scenarios, the sensitivity and specificity are close to the accuracy rates. It is worth noting that extracting Gabor features in the CXR spatial domain achieved significantly lower accuracy for the same experimental data set. These results reveal that the Gabor filtering in the LBP transform uncovers all significantly visible texture features in infected CXRs throughout the chest that are not limited to the ribs or the chest cage bones. The additional visible features are reflected as artefacts that must have been caused by X-Rays' detectible infection-caused changes in the chest and airways. These observations are clearly illustrated in the appendix displayed images, especially in the off-diagonal top-left Gabor sub-images. These artefacts are not hardly visible in the normal CXRs. Moreover, we observe notable differences in the extent of additional artefacts between the CXR's of COVID-19 infected patients from those of the patients exhibiting viral and bacterial infection. These observations, if further confirmed, maybe useful in providing the clinician with convincing evidence of the LBP-Gabor scheme predicted decision by complementing our interface software with a visual display of some of the created sub-images.

The results in Table II for the prospective tests follow the same pattern described above, but in all cases, there is a tolerable reduction in accuracy for all scenarios. This reduction can be explained by the fact that none of the images in the prospective datasets is involved in the training/testing of the SVM model. The fact that all features were extracted directly from the LBP images with image enhancement and de-noising, demonstrate the success of strategy of texture analysis in the LBP transform domain. It is worth noting that, we test a larger number of LBP-texture schemes and most of the unpresented schemes achieved in-excess of 80% accuracy.

V. CONCLUSION AND FUTURE WORK

This paper investigated and evaluated the proposed innovative approach of extracting texture features from the LBP-transformed CXR images of different types of chest infections, with the aim of developing an automatic CAD system to be used for distinguishing between COVID-19 and non-COVID-19. This paper is a follow up on our COVID-19 infection detection by texture analysis CT scan images where the FFT-Gabor scheme achieved accuracy in-excess of 95%. The choice of using CXR instead of CT (standard and low dose) is due to the significant differences in the harmful ionizing radiation dose (0.1 mSv for CXR compared to 7 mSv for standard CT and 1.5 mSv for LDCT). Consequently, CXR is a much safer option.

Experimental test results over different collected sufficiently large datasets show that the corresponding SVM models built on several texture features extracted from the LBP domain achieved accuracy well above random guess (minimum 75%). The LBP-Gabor filters attained the highest and stable accuracy of 94.15% with equally impressive near equal sensitivity and

specificity rates. Decision level fusion of all texture features resulted in average accuracies close to 95%, and higher than those by the individual features. These results demonstrate the viability and effectiveness of the LBP transform domain to extracted features for the stated task. We have also observed the possibility of using the LBP-Gabor filtered sub-images as an additional visual evidence of the predicted decision within clinical setting. Due to the promising results, we are currently testing LBP-Gabor and FFT-Gabor texture features for lung tumor detection.

APPENDIX

Figs. 5-9 are an illustration of the output of using the LBP-Gabor scheme that filters the LBP transformed images (1 Normal, 2 COVID-19, 1 Virus and 1 Bacteria) in 2 scales and 1 orientation. It is easy to visibly note the differences in the pattern displayed in each of the 50 small LBP-Gabor blocks between the COVID-19 and normal cases. Such displays provide the clinician and informative justification of the output decision.

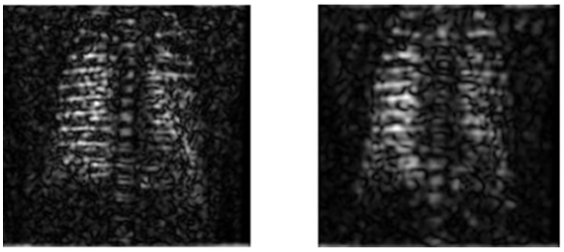

Fig. 5 An example of using LBP-Gabor scheme on Normal

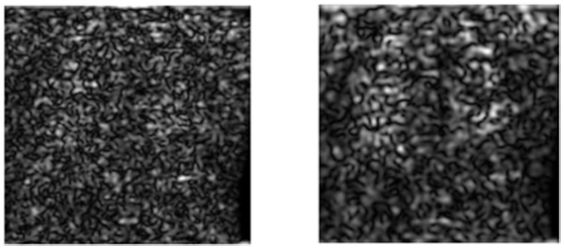

Fig. 6 An example of using LBP-Gabor scheme on COVID-19 CXR image

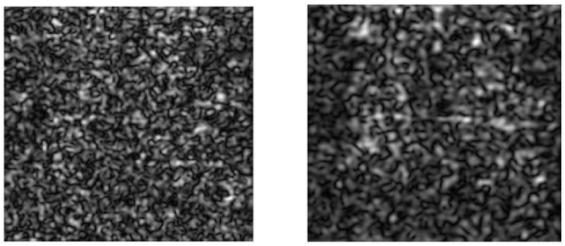

Fig. 7 An example of using LBP-Gabor scheme on COVID-19 CXR image

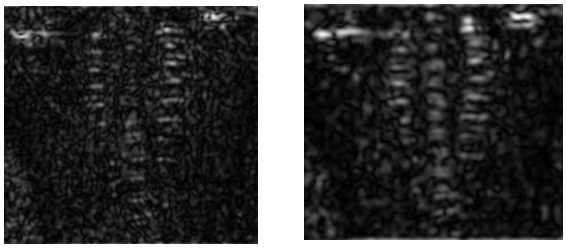

Fig. 8 An example of using LBP-Gabor scheme on Virus CXR image

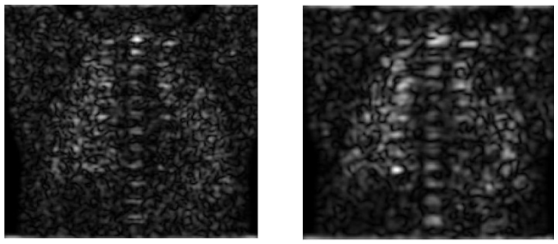

Fig. 9 An example of using LBP-Gabor scheme on Bacteria CXR image

REFERENCES

[1] ""European Centre for Disease Prevention and Control, situation update worldwide," (Online). Available: https://www.ecdc.europa.eu/en/geographical-distribution-2019-ncov-cases. (Accessed 22 06 2020).

[2] "Guidance and standard operating procedure: COVID-19 virus testing in NHS laboratories," (Online). Available: https://www.england.nhs.uk/coronavirus/publication/guidance-and-standard-operating-procedure-covid-19-virus-testing-in-nhs-laboratories/. (Accessed 01 05 2020).

[3] T. Ai, Z. Yang, H. Hou, C. Zhan, C. Chen, W. Lv, Q. Tao, Z. Sun and L. Xia, "Correlation of chest CT and RT-PCR testing in coronavirus disease 2019 (COVID-19) in China: a report of 1014 cases," Radiology, p. 200642, 2020.

[4] Y. Li, L. Yao, L. Chen, Y. Song and others, "Stability Issues of RT-PCR Testing of SARS-CoV-2 for Hospitalized Patients Clinically Diagnosed with COVID-19," Journal of Medical Virology, 2020.

[5] T. R. Group, "Roche develops new serology test to detect COVID-19 antibodies," April 2020. (Online). Available: https://www.roche.com/media/releases/med-cor-2020-04-17.htm. (Accessed 31 06 2020).

[6] The Guardian, "WHO warns that few have developed antibodies to Covid-19," 01 06 2020. (Online). Available: https://www.theguardian.com/society/2020/june/01/studies-suggest-very-few-have-had-covid-19-without-symptoms.

[7] buzzfeednews, "Two Antibody Studies Say Coronavirus Infections Are More Common Than We Think. Scientists Are Mad.," 22 05 2020. (Online). Available: https://www.buzzfeednews.com/article/stephaniemlee/coronavirus-antibody-test-santa-clara-los-angeles-stanford.

[8] G. D. Rubin, C. J. Ryerson, L. B. Haramati, N. Sverzellati, J. P. Kanne and others, "The role of chest imaging in patient management during the COVID-19 pandemic: a multinational consensus statement from the Fleischner Society," Chest, 2020.

[9] A. Nair, J. Rodrigues, S. Hare, A. Edey, A. Devaraj, J. Jacob, A. Johnstone, R. McStay, E. Denton and G. Robinson, "A British Society of Thoracic Imaging statement: considerations in designing local imaging diagnostic algorithms for the COVID-19 pandemic," Clinical Radiology, vol. 75, pp. 329--334, 2020.

[10] H. Wong, H. Y. S. Lam, A. Fong, S. T. Leung and o. Chin, "Frequency and distribution of chest radiographic findings in COVID-19 positive patients," Radiology, p. 201160, 2020.

[11] I. Castiglioni, D. Ippolito, M. Interlenghi, C. B. Monti, C. Salvatore, S. Schiaffino, A. Polidori and others, "Artificial intelligence applied on chest X-ray can aid in the diagnosis of COVID-19 infection: a first experience from Lombardy, Italy," medRxiv, 2020.

[12] E. E.-D. Hemdan, M. A. Shouman and M. E. Karar, "Covidx-net: A framework of deep learning classifiers to diagnose covid-19 in x-ray images," arXiv preprint arXiv:2003.11055, 2020.
[13] M. Ilyas, H. Rehman and A. Nait-ali, "Detection of Covid-19 From Chest X-ray Images Using Artificial Intelligence: An Early Review," arXiv preprint arXiv:2004.05436, 2020.
[14] D. Al-Karawi, S. Al-Zaidi, N. Polus and S. Jassim, "Machine Learning Analysis of Chest CT Scan Images as a Complementary Digital Test of Coronavirus (COVID-19) Patients," medRxiv, 2020.
[15] D. Camilleri and T. Prescott, "Analysing the limitations of deep learning for developmental robotics," in conference on Biomimetic and Biohybrid Systems, Springer, 2017, pp. 86--94.
[16] D. Al-Karawi, C. Landolfo, H. Du, H. Al-Assam, A. Sayasneh, D. Timmerman, T. Bourne and S. Jassim, "OC04. 04: A machine-learning algorithm to distinguish benign and malignant adnexal tumours from ultrasound images," Ultrasound in Obstetrics & Gynecology, vol. 54, pp. 9--10, 2019.
[17] D. Al-karawi, A. Sayasneh, H. Al-Assam, S. Jassim, N. Page, D. Timmerman, T. Bourne and H. Du, "An automated technique for potential differentiation of ovarian mature teratomas from other benign tumours using neural networks classification of 2D ultrasound static images: a pilot study," in Mobile Multimedia/Image Processing, Security, and Applications 2017, International Society for Optics and Photonics, 2017, p. 102210F.
[18] C. Cortes and V. Vapnik, "Support-vector networks," Machine learning, vol. 20, pp. 273--297, 1995.
[19] M. S. Nixon and A. S. Aguado, Feature extraction & image processing for computer vision, Academic Press, 2012.
[20] J. Ilonen and J.-K. a. o. Kamarainen, "Image feature localization by multiple hypothesis testing of Gabor features," IEEE Transactions on Image Processing, vol. 17, pp. 71--82, 2008.
[21] T. M. P. a. D. H. Ojala, "A comparative study of texture measures with classification based on featured distributions," Pattern recognition, Elsevier, pp. 51-59, 1996.
[22] N. Dalal and B. Triggs, "Histograms of oriented gradients for human detection," in 2005 IEEE computer society conference on computer vision and pattern recognition (CVPR'05), vol. 1, IEEE, 2005, pp. 886--893.
[23] "https://github.com/ieee8023/covid-chestxray-dataset/tree/master/images," (Online). (Accessed 30 06 2020).
[24] "https://data.mendeley.com/datasets/rscbjbr9sj/3," (Online). (Accessed 05 04 2020).